

UCLA

UCLA Previously Published Works

Title

18F-FAC PET Visualizes Brain-Infiltrating Leukocytes in a Mouse Model of Multiple Sclerosis.

Permalink

<https://escholarship.org/uc/item/3cf109h4>

Journal

Journal of nuclear medicine : official publication, Society of Nuclear Medicine, 61(5)

ISSN

0161-5505

Authors

Chen, Bao Ying
Ghezzi, Chiara
Villegas, Brendon
et al.

Publication Date

2020-05-01

DOI

10.2967/jnumed.119.229351

Peer reviewed

^{18}F -FAC PET visualizes brain-infiltrating leukocytes in a mouse model of multiple sclerosis

Bao Ying Chen^{1,2}, Chiara Ghezzi^{1,2}, Brendon Villegas³, Andrew

Quon^{1,4}, Caius G. Radu^{1,4}, Owen N. Witte^{1,5,6}, Peter M. Clark^{1,2,5,†}

¹ Department of Molecular and Medical Pharmacology, ² Crump Institute for Molecular Imaging, ³ Department of Pulmonary and Critical Care Medicine, ⁴ Ahmanson Translational Imaging Division, ⁵ Eli and Edythe Broad Center of Regenerative Medicine and Stem Cell Research, ⁶ Department of Microbiology, Immunology, and Molecular Genetics, University of California, Los Angeles, CA 90095.

‡ Correspondence should be addressed to Peter M. Clark, Crump Institute, Box 951770, 4333 CNSI, Los Angeles, CA 90095-1770; 310-267-4755; pclark@mednet.ucla.edu

First author: Bao Ying Chen, Crump Institute, Box 951770, 4333 CNSI, Los Angeles, CA 90095-1770; 310-267-4755; BaoYingChen@mednet.ucla.edu (Graduate student)

Word count: 4,976

Financial support: This work was supported by the UCLA Eugene Cota Robles Fellowship (to BYC), NIH grant R21AI119916 (to PMC), NIH grant R01NS112287 (to PMC), Parker Institute for Cancer Immunotherapy grant 20163828 (to ONW), and by the Broad Stem Cell Research Center at UCLA. ONW and CGR are inventors on a patent held by the University of California Regents that discloses ^{18}F -FAC. There are no other potential conflicts of interest.

Running title: Imaging brain leukocytes with ^{18}F -FAC

ABSTRACT

Brain-infiltrating leukocytes contribute to multiple sclerosis (MS) and autoimmune encephalomyelitis and likely play a role in traumatic brain injury, seizure, and stroke. Brain-infiltrating leukocytes are also primary targets for MS disease-modifying therapies. However, no method exists for non-invasively visualizing these cells in a living organism. 1-(2'-deoxy-2'- ^{18}F -fluoroarabinofuranosyl) cytosine (^{18}F -FAC) is a PET radiotracer that measures deoxynucleoside salvage and accumulates preferentially in immune cells. We hypothesized that ^{18}F -FAC PET could non-invasively image brain-infiltrating leukocytes. **Methods** Healthy mice were imaged with ^{18}F -FAC PET to quantify if this radiotracer crosses the blood-brain barrier (BBB). Experimental autoimmune encephalomyelitis (EAE) is a mouse disease model with brain-infiltrating leukocytes. To determine whether ^{18}F -FAC accumulates in brain-infiltrating leukocytes, EAE mice were analyzed with ^{18}F -FAC PET, digital autoradiography, and immunohistochemistry, and ^{18}F -FAC accumulation in brain-infiltrating leukocytes was analyzed *ex vivo*. Fingolimod-treated EAE mice were imaged with ^{18}F -FAC PET to assess if this approach can monitor the effect of an immunomodulatory drug on brain-infiltrating leukocytes. PET scans of individuals injected with 2-chloro-2'-deoxy-2'- ^{18}F -fluoro-9- β -D-arabinofuranosyl-adenine (^{18}F -CFA), a PET radiotracer that measures deoxynucleoside salvage in humans, were analyzed to evaluate whether ^{18}F -CFA crosses the human BBB. **Results** ^{18}F -FAC accumulates in the healthy mouse brain at similar levels to ^{18}F -FAC in the blood (2.54 ± 0.2 and 3.04 ± 0.3 %ID/g, respectively) indicating that ^{18}F -FAC crosses the BBB. EAE mice accumulate ^{18}F -FAC in the brain at 180% of the levels of control mice. Brain ^{18}F -FAC accumulation localizes to periventricular regions with significant leukocyte infiltration, and ^{18}F -FAC accumulates at similar levels in brain-infiltrating T and innate immune cells. These data suggest that ^{18}F -FAC accumulates in brain-infiltrating leukocytes in this model. Fingolimod-treated EAE mice accumulate ^{18}F -FAC in the brain at 37% lower levels than control-treated EAE mice demonstrating that ^{18}F -FAC PET can monitor therapeutic interventions in this

mouse model. ^{18}F -CFA accumulates in the human brain at 15% of blood levels (0.08 ± 0.01 and 0.54 ± 0.07 SUV, respectively), indicating that ^{18}F -CFA does not cross the BBB in humans.

Conclusions ^{18}F -FAC PET can visualize brain-infiltrating leukocytes in a mouse MS model and can monitor the response of these cells to an immunomodulatory drug. Translating this strategy into humans will require exploring additional radiotracers.

Key words: PET imaging, autoimmune disease, leukocytes, brain

INTRODUCTION

Brain-infiltrating leukocytes drive pathology in multiple sclerosis (MS) and autoimmune encephalomyelitis (1–4). During MS, brain-infiltrating T cells, B cells, and macrophages promote neurodegeneration (1–3), and disease-modifying therapies modulate the immune system (4). Leukocytes are also found in the brains of murine models of traumatic brain injury, stroke, and seizure and of postmortem Parkinson's disease and P301L tau frontotemporal dementia patients (5–12). Inhibiting leukocyte migration into the brain or depleting lymphocytes in these animal models can slow disease progression (6–12), suggesting a functional role for the immune system in these diseases. Although PET assays have been developed to image and quantify different aspects of neuroinflammation (13–17), there is no PET assay to visualize brain-infiltrating leukocytes. A non-invasive method to selectively image and quantify brain-infiltrating leukocytes would complement current approaches and provide information on the location of these cells during the development and treatment of neurological diseases.

The radiotracer 1-(2'-deoxy-2'-¹⁸F-fluoroarabinofuranosyl) cytosine (¹⁸F-FAC) is a deoxynucleoside analogue that measures deoxynucleoside salvage, a biochemical pathway enriched in leukocytes; accumulates at high levels in lymphoid tissues; and is increased in these same tissues in mouse models of immune activation (18–20). Additionally, ¹⁸F-FAC accumulates at higher levels in activated T lymphocytes than in effector-memory T cells, CD11b⁺ innate immune cells, or B220⁺ B cells and at low levels in the healthy brain (18–20). Thus we hypothesized that ¹⁸F-FAC PET could non-invasively visualize brain-infiltrating leukocytes.

Here we study ¹⁸F-FAC in an experimental autoimmune encephalomyelitis (EAE) mouse model of MS. Our results suggest that ¹⁸F-FAC PET can visualize brain-infiltrating leukocytes during disease and treatment.

MATERIALS AND METHODS

Mice

10 week old, female C57BL/6N and NOD.Cg-*Prkdc*^{scid} *Il2rg*^{tm1Wjl}/SzJ (NSG) mice were used for all experiments. All mouse experiments were approved by the UCLA Animal Resource Committee.

Treatments

EAE treatments were conducted and scored similar to reported (15,21). Briefly, mice were injected with an emulsion of myelin oligodendrocyte glycoprotein (MOG₃₅₋₅₅) in Freund's complete adjuvant (100 μ L) and with pertussis toxin (80 ng) 2 hours and again 24 hours later (Hooke Laboratories). All experiments were conducted 13 to 15 days post-immunization. Fingolimod (0.5 mg/kg; Selleckchem S5002) or vehicle were injected intraperitoneal daily starting immediately post-immunization. Immunocompetent EAE mice were used at an average clinical score of 3.0.

Immunohistochemical Analyses

Sagittal brain sections (4 μ m) were immunostained as described (20) except for the inclusion of CD45 (Clone 30-F11; 1:100; Novus Biologicals), imaged at 1X and 40X magnification, and quantified using the Ilastik software (Version 1.3.2). Boxes in the 1x magnification images outline from where the 40x magnification images were taken. To evaluate correlations, two independent 40X magnification images were scored using an H-score (22).

¹⁸F-FAC PET/CT

Mice injected with either ¹⁸F-FAC (1.85 MBq) or with ¹⁸F-FAC (1.85 MBq) and 10 mg of non-radiolabeled FAC were imaged for an hour or imaged one hour post-injection for 10 min on a G8 PET/CT. The one hour post-injection time point was chosen as this is the earliest time point at which ¹⁸F-FAC accumulation in the brain and blood no longer rapidly changes. Images were

analyzed using AMIDE (Version 1.0.4), and the MRM neurological atlas was fitted to the mouse skull (23,24). Regions of interest (ROI) were drawn at the interface of the hippocampus, thalamus, and midbrain as demarcated by the neurological atlas. ^{18}F -FAC blood levels were determined from a ROI drawn within the left ventricle of the heart.

^{18}F -CFA PET Analysis

^{18}F -CFA PET scans from (25) were analyzed. ROI were drawn similar to the mouse PET/CT images.

***Ex vivo* Biodistribution Studies**

Mice were injected with ^{18}F -FAC (1.85 MBq). One hour post-injection, blood (100 μL) was collected, the mice were perfused, and organs were extracted and rinsed in 1x PBS. Activity and weight of the blood and organs were measured.

Autoradiography

Autoradiography was performed as previously described (26). Briefly, pre- and post-immunization EAE mice were injected with ^{18}F -FAC (18.5 MBq) and sagittal brain sections (10 μm) from perfused mice were cut.

***Ex vivo* Accumulation Assays**

Brain leukocyte isolation was conducted similar to previously described (27), and CD4^+ and CD11b^+ cells were isolated by FACS. *Ex vivo* deoxycytidine accumulation was performed as previously described (20) by incubating ~20,000 of each cell type in a 96-well filter plate with ^3H -deoxycytidine (0.037 MBq per well) for 30 min.

Statistical Analyses

Data was analyzed using GraphPad Prism (Version 7.03). Statistical comparisons were performed using two-sided *t*-tests and one-way ANOVA analyses with multiple comparison testing. Data is reported as mean \pm standard error.

RESULTS

¹⁸F-FAC Crosses the Healthy BBB in Mice

To develop a PET assay to quantify brain-infiltrating leukocytes in neurological diseases, we needed a PET radiotracer that accumulates in leukocytes and crosses the BBB. ¹⁸F-FAC is a pyrimidine deoxynucleoside analogue radiotracer that accumulates in leukocytes (18,19). Generally, pyrimidine ribonucleosides except for uridine do not cross the BBB, but studies suggest that ¹⁸F-FAC accumulates at ~ 2 %ID/g in the brain of healthy mice (18,28).

¹⁸F-FAC accumulated at nearly uniform levels throughout the healthy mouse brain as evaluated by PET and autoradiography one hour post-injection (Fig. 1A, B). ¹⁸F-FAC levels in the healthy mouse brain, corrected for blood volume in the brain (29), were slightly lower than ¹⁸F-FAC levels in the blood (brain-to-blood ratio quantified from the PET images: 0.84 ± 0.05 – brain: 2.54 ± 0.2 %ID/g, blood: 3.04 ± 0.3 %ID/g; brain-to-blood ratio quantified from isolated tissue and blood: 0.76 ± 0.05 ; Figs. 1C, D; ¹⁸F-FAC time-activity curves: Supplemental Fig. 1; correlation between brain-to-blood ratios quantified from the PET images and from isolated tissue and blood: $R^2 = 0.89$, Supplemental Fig. 2). ¹⁸F-FAC has a logP value of -1.33, well below the 2 – 3.5 logP value of most radiotracers that diffuse into the brain and suggesting that ¹⁸F-FAC is transported across the BBB (30). Collectively, these data suggest that ¹⁸F-FAC crosses the healthy BBB.

Brain-Infiltrating Leukocytes are Present in an EAE Mouse Model

EAE is a well-established MS model with leukocyte infiltration into the spinal cord and brain (31,32). EAE was induced in immunocompetent C57BL/6 and immunocompromised NSG mice by co-injecting MOG₃₅₋₅₅ in Freund's complete adjuvant with pertussis toxin (15,21). Consistent with literature (15,21), immunocompetent mice began to display EAE symptoms ~9 days post-immunization that peaked ~13 days post-immunization and which included a limp tail, hind leg paralysis, and severe head tilting (Fig. 2A). Immunocompromised mice treated to induce EAE never displayed symptoms (Fig. 2A). Immunohistochemistry of immunocompetent mouse brain sections demonstrated significant perivascular and periventricular leukocyte infiltrates characterized by an abundance of CD11b-positive innate immune cells and CD4 T cells with few B220-positive B cells and CD8 T cells (Fig. 2B). $37 \pm 2\%$ of infiltrating leukocytes in these sections were dividing as suggested by Ki67 immunostaining. No infiltrating leukocytes were observed in the immunocompromised EAE mouse brains (Fig. 2B). Isolated leukocytes from immunocompetent EAE mouse brains were similarly enriched for CD11b-positive innate immune cells and CD4 T cells (Fig. 2C).

¹⁸F-FAC Accumulates at Higher Levels in the Brains of EAE Mice than Control Mice

Immunocompetent and immunocompromised pre-immunization and EAE mice were injected with ¹⁸F-FAC and imaged by PET/CT one hour later. ¹⁸F-FAC accumulation in the brains of immunocompetent EAE mice was 180% of the levels of pre-immunization immunocompetent mice based on a ROI drawn at the interface of the hippocampus, midbrain, and thalamus where a high concentration of infiltrating leukocytes resides (pre-immunization immunocompetent mice: 2.4 ± 0.15 %ID/g; immunocompetent EAE mice: 4.4 ± 0.66 %ID/g; Fig. 3A; Supplemental Fig. 3). ¹⁸F-FAC accumulation in this same brain region of immunocompromised EAE mice was not

significantly different from pre-immunization immunocompromised mice (pre-immunization immunocompromised mice: 3.2 ± 0.31 %ID/g; immunocompromised EAE mice: 2.4 ± 0.15 %ID/g; Fig. 3B; Supplemental Fig. 3). ^{18}F -FAC brain accumulation was lower in immunocompetent mice than in immunocompromised mice pre-immunization, and lower in post-immunization than in pre-immunization immunocompromised mice. We cannot readily explain either of these results, although neither result reached statistical significance. ^{18}F -FAC accumulation was also significantly increased in the spleen and lymph nodes but not the femur, bone marrow, or spinal cord of the immunocompetent EAE compared to pre-immunization mice (quantified from the PET images: spleen – pre-immunization mice: 11.8 ± 2.1 %ID/g, EAE mice: 21.3 ± 3.2 %ID/g; lymph nodes – pre-immunization mice: 2.3 ± 0.06 %ID/g, EAE mice: 9.1 ± 0.84 %ID/g; bone marrow – pre-immunization mice: 14.7 ± 1.1 %ID/g, EAE mice: 11.9 ± 1.5 %ID/g; spinal cord – pre-immunization mice: 4.9 ± 0.24 %ID/g, EAE mice: 5.7 ± 0.70 %ID/g; Supplemental Fig. 4; *ex vivo* biodistribution data: Supplemental Fig. 5).

EAE mice suffer BBB breakdown, leading to the slow exchange or pooling of blood fluids in areas with significant leukocyte infiltration and a compromised BBB (33). Our results in the EAE model could be due to ^{18}F -FAC in these blood pools and not to specific cellular ^{18}F -FAC accumulation. Immunocompetent EAE mice were injected with ^{18}F -FAC supplemented with 10 mg non-radiolabeled FAC. Cellular FAC accumulation can be saturated but FAC accumulation in blood pools cannot. Co-injection of ^{18}F -FAC and non-radiolabeled FAC decreased brain ^{18}F -FAC accumulation in immunocompetent EAE mice by 57% compared to immunocompetent EAE mice injected with only ^{18}F -FAC and to 78% of the levels of pre-immunization immunocompetent mice (pre-immunization immunocompetent mice: 2.4 ± 0.15 %ID/g; immunocompetent EAE mice: 4.4 ± 0.66 %ID/g; immunocompetent EAE mice injected with ^{18}F -FAC and non-radiolabeled FAC: 1.9 ± 0.15 %ID/g; Fig. 3A; Supplemental Fig. 3). This suggests that the increased ^{18}F -FAC

accumulation in the immunocompetent EAE mouse brains is due to specific cellular ^{18}F -FAC accumulation.

^{18}F -FAC Accumulates in Brain-Infiltrating Leukocytes in an EAE Mouse Model

Deoxycytidine kinase (dCK) phosphorylates ^{18}F -FAC and is a rate-limiting enzyme in the cellular accumulation of this radiotracer (18,34). Brain sections of pre-immunization or EAE mice were immunostained with an antibody targeting dCK. Strong dCK immunostaining was apparent in $68\pm5\%$ of the infiltrating leukocytes in the brain sections of the immunocompetent EAE mice and the intensity and number of immunostained leukocytes correlated with brain ^{18}F -FAC accumulation ($R^2=0.85$; Fig. 4A; Supplemental Fig. 6). In contrast, $37\pm12\%$ of leukocytes in the spinal cord of immunocompetent EAE mice, a tissue in which ^{18}F -FAC accumulation did not increase compared to pre-injection mice, stained strongly for dCK (Supplemental Fig. 7). Weak dCK immunostaining was present in the brain parenchyma across all conditions, and the degree of dCK immunostaining in the brain parenchyma was unaffected by the EAE treatment (Fig. 4A). This suggests increased brain ^{18}F -FAC accumulation in the immunocompetent EAE mice may be due to the tracer accumulating in the brain-infiltrating leukocytes. Consistent with this model, autoradiography of brain sections of immunocompetent EAE mice injected with ^{18}F -FAC shows the greatest enrichment in ^{18}F -FAC accumulation specifically in areas coincident with significant leukocyte infiltration in the EAE mouse brain (Fig. 4B).

Brain-infiltrating leukocytes in this model consist mostly of CD11b-positive innate immune cells and CD4 T cells (Fig. 2B, C). Deoxynucleoside salvage activity was similar between CD11b-positive innate immune cells and CD4 T cells isolated from the immunocompetent EAE mouse brains (Fig. 4C). Insufficient B220-positive B cells and CD8 T cells could be isolated for analysis. The number of leukocytes in the brain correlated with ^{18}F -FAC accumulation ($R^2=0.82$;

Supplemental Fig. 8). Whether activated microglia also consume ^{18}F -FAC remains a topic for future study. However the overlap between the strong ^{18}F -FAC accumulation identified in the autoradiography and the areas identified by immunohistochemistry as having significant leukocyte infiltration (Figs. 2B, 4B) supports our interpretation that ^{18}F -FAC accumulates in and ^{18}F -FAC PET images brain-infiltrating leukocytes. Collectively this suggests a model in which elevated ^{18}F -FAC accumulation in brain regions of immunocompetent EAE mice with significant leukocyte infiltration is due to ^{18}F -FAC accumulation in all of the brain-infiltrating leukocyte populations.

Changes in Brain ^{18}F -FAC Accumulation can Monitor Immunomodulatory Drug Treatments in EAE Mice

The small molecule fingolimod modulates the sphingosine-1-phosphate receptor, sequesters lymphocytes in lymph nodes and the spleen, and limits autoimmune diseases such as MS (4,35). Fingolimod decreased leukocytes in the brain of immunocompetent EAE mice compared to vehicle treatment (Fig. 5A). Fingolimod also significantly decreased brain ^{18}F -FAC accumulation compared to vehicle treatment in these same mice (pre-immunization mice: 2.0 ± 0.13 %ID/g, EAE mice treated with vehicle: 4.2 ± 0.25 %ID/g, EAE mice treated with fingolimod: 2.7 ± 0.08 %ID/g; Fig. 5B, Supplemental Fig. 3). Consistent with its mechanism of sequestering lymphocytes to lymph nodes and the spleen (4,35), fingolimod had no effect on ^{18}F -FAC accumulation in the lymph nodes and spleen of immunocompetent EAE mice (lymph nodes – EAE mice: 9.1 ± 0.84 %ID/g, EAE mice treated with fingolimod: 6.5 ± 0.26 %ID/g; Spleen – EAE mice: 21.3 ± 3.2 %ID/g, EAE mice treated with fingolimod: 26.2 ± 1.8 %ID/g; Supplemental Fig. 3, Supplemental Fig. 4).

¹⁸F-CFA does not Cross the BBB in Humans

¹⁸F-FAC is deaminated in humans but 2-chloro-2'-deoxy-2'-¹⁸F-fluoro-9-β-D-arabinofuranosyl-adenine (¹⁸F-CFA), a radiotracer that also measures deoxynucleoside salvage, is not (36–38). Accounting for blood volume in the brain (39), ¹⁸F-CFA accumulates in the brain at 11.0±1.4% of the levels of ¹⁸F-CFA found in the blood (135 min post-injection: brain SUV: 0.08±0.01; blood SUV: 0.54±0.07; Supplemental Fig. 9), suggesting that ¹⁸F-CFA does not cross the BBB in healthy human patients.

DISCUSSION

Despite studies showing that ¹⁸F-FAC selectively accumulates in activated lymphocytes in mouse models of autoimmune hepatitis and antitumor immunity (18–20), in the EAE mouse model we do not identify selective ¹⁸F-FAC accumulation in brain-infiltrating lymphocytes. In the mouse model of antitumor immunity, the rate of ¹⁸F-FAC accumulation in T cells was proportional to the rate of cellular proliferation (19). One explanation for our results is that brain-infiltrating lymphocytes are not rapidly dividing and thus do not consume high ¹⁸F-FAC levels. Only 37±2% of the brain-infiltrating leukocytes in our model are dividing, similar to the number of dividing liver-infiltrating leukocytes in a viral hepatitis model in which no enhanced hepatic ¹⁸F-FAC accumulation was observed (20). ¹⁸F-FAC is likely able to image infiltrating leukocytes in the EAE model but not the viral hepatitis model due to the ~50% lower basal accumulation of ¹⁸F-FAC in the brain than the liver. ¹⁸F-FAC may show selectivity for lymphocytes in other models with more actively dividing lymphocytes in the brain.

We show higher ¹⁸F-FAC accumulation in brain-infiltrating leukocytes and in lymphoid organs such as the spleen and lymph nodes in the EAE model. ¹⁸F-FAC measures deoxynucleoside salvage, for which dCK is a rate-limiting enzyme, and genetic knockout of dCK

in healthy mice leads to decreased lymphocyte levels (18,34). Small molecule dCK inhibitors with *in vivo* efficacy have been developed (40). Our data may suggest that dCK inhibitors could limit disease in this model.

A previous study found that ^{18}F -FDG accumulation in the spinal cord increased by 200% compared to control mice in this exact EAE model at the exact time point we studied (15). We identify no significant increase in spinal cord ^{18}F -FAC accumulation in the EAE mice, suggesting that in this model, immune cells in the spinal cord increase glucose but not deoxynucleoside consumption. This result is supported by the lower percentage of leukocytes in the spinal cord relative to the brain of EAE mice that stain strongly for dCK. This data suggesting that immune cells at different anatomical locations have different metabolic needs is consistent with data showing a much larger increase in ^{18}F -FDG than ^{18}F -FAC consumption in the draining lymph nodes of a mouse rhabdomyosarcoma model (19).

Implications for Human Studies

Brain-infiltrating leukocytes contribute to neurological diseases, and MS and possibly other neurological diseases can be treated with immunomodulatory drugs (1–9). Many immunomodulatory drugs cause significant side effects, and in MS the primary effects of these drugs on the immune system are assessed indirectly with MRI and clinical evaluations (41). PET assays with radiotracers that measure deoxynucleoside salvage could directly monitor the effect of these drugs on brain-infiltrating leukocytes. We demonstrate how this might work with the drug fingolimod.

Both ^{18}F -FAC and ^{18}F -CFA measure deoxynucleoside salvage (18,38). ^{18}F -CFA works poorly in mice due to high plasma deoxycytidine levels but is resistant to deamination in humans (37,38). However ^{18}F -CFA does not cross the BBB in humans, suggesting that a different radiotracer will need to be tested in humans. These could include the ^{18}F -FAC derivatives L- ^{18}F -

FAC and 2'-deoxy-2'-¹⁸F-fluoro-5-methyl-β-L-arabinofuranosylcytosine, which are resistant to deamination (36). Additional studies would have to be conducted with these radiotracers to determine whether they cross the human BBB.

CONCLUSION

This study suggests that ¹⁸F-FAC PET can non-invasively image brain-infiltrating leukocytes and can function as a pharmacodynamic biomarker of drugs that modulate these cells in mice. However, PET tracers that measure deoxynucleoside salvage and cross the BBB in humans will need to be further explored. We and others have shown that PET with radiotracers that measure deoxynucleoside salvage can image the immune system at least preclinically in various autoimmune conditions (18,20,42). The consistent activation of deoxynucleoside salvage in all of these settings may suggest a larger role for inhibitors of this pathway and a universal strategy for monitoring therapeutic responses in autoimmune disease.

DISCLOSURES

This work was supported by the UCLA Eugene Cota Robles Fellowship (to BYC), NIH grant R21AI119916 (to PMC), NIH grant R01NS112287 (to PMC), Parker Institute for Cancer Immunotherapy grant 20163828 (to ONW), and by the Broad Stem Cell Research Center at UCLA. ONW and CGR are inventors on a patent held by the University of California Regents that discloses ¹⁸F-FAC. There are no other potential conflicts of interest.

ACKNOWLEDGEMENTS

We thank the Crump Cyclotron and Radiochemistry Technology Center, the Crump Institute Preclinical Imaging Technology Center, the Translational Pathology Core Laboratory, and the Center for AIDS Research Flow Cytometry Core Facility at UCLA. We thank Eva Koziolk for tail vein injections. We thank Ralph and Marjorie Crump for their generous gift to the Crump Institute for Molecular Imaging.

KEY POINTS

QUESTION:

- Can PET imaging with ^{18}F -FAC, which measures deoxynucleoside salvage, visualize brain-infiltrating leukocytes, a cell population that can contribute to neurological disease pathology and may serve as an important therapeutic target?

PERTINENT FINDINGS:

- ^{18}F -FAC accumulates in the brains of a MS mouse model at 180% of the levels found in the brains of control mice, and ^{18}F -FAC accumulates in areas of significant leukocyte infiltration and at nearly equal levels in brain-infiltrating T cells and innate immune cells.
- ^{18}F -FAC accumulation in the brains of these mice decreases by 37% when they are treated with the immunomodulatory drug fingolimod, suggesting that changes in brain ^{18}F -FAC accumulation can monitor a therapy in this model.

IMPLICATIONS FOR PATIENT CARE:

- A PET assay with a radiotracer that measures the deoxynucleoside salvage pathway may image brain-infiltrating leukocytes in patients with neurological disease and during therapeutic interventions.

REFERENCES

1. Compston A, Coles A. Multiple sclerosis. *Lancet*. 2008;372:1502-1517.
2. Dendrou CA, Fugger L, Friese MA. Immunopathology of multiple sclerosis. *Nat Rev Immunol*. 2015;15:545-558.
3. Traugott U, Reinherz EL, Raine CS. Multiple sclerosis: distribution of T cell subsets within active chronic lesions. *Science*. 1983;219:308-310.
4. Wingerchuk DM, Carter JL. Multiple sclerosis: current and emerging disease-modifying therapies and treatment strategies. *Mayo Clin Proc*. 2014;89:225-240.
5. Bai R, Gao H, Han Z, et al. Long-term kinetics of immunologic components and neurological deficits in rats following repetitive mild traumatic brain injury. *Med Sci Monit*. 2017;23:1707-1718.
6. Ertürk A, Mentz S, Stout EE, et al. Interfering with the chronic immune response rescues chronic degeneration after traumatic brain injury. *J Neurosci*. 2016;36:9962-9975.
7. Brochard V, Combadière B, Prigent A, et al. Infiltration of CD4+ lymphocytes into the brain contributes to neurodegeneration in a mouse model of Parkinson disease. *J Clin Invest*. 2009;119:182-192.
8. Laurent C, Dorothée G, Hunot S, et al. Hippocampal T cell infiltration promotes neuroinflammation and cognitive decline in a mouse model of tauopathy. *Brain J Neurol*. 2017;140:184-200.
9. Dong T, Zhi L, Bhayana B, Wu MX. Cortisol-induced immune suppression by a blockade of lymphocyte egress in traumatic brain injury. *J Neuroinflammation*. 2016;13:197.
10. Yilmaz G, Arumugam TV, Stokes KY, Granger DN. Role of T lymphocytes and interferon-gamma in ischemic stroke. *Circulation*. 2006;113:2105-2112.
11. Grønberg NV, Johansen FF, Kristiansen U, Hasseldam H. Leukocyte infiltration in experimental stroke. *J Neuroinflammation*. 2013;10:115.
12. Varvel NH, Neher JJ, Bosch A, et al. Infiltrating monocytes promote brain inflammation and exacerbate neuronal damage after status epilepticus. *Proc Natl Acad Sci U S A*. 2016;113:E5665-5674.
13. Airas L, Dickens AM, Elo P, et al. In vivo PET imaging demonstrates diminished microglial activation after fingolimod treatment in an animal model of multiple sclerosis. *J Nucl Med*. 2015;56:305-310.
14. Unterrainer M, Mahler C, Vomacka L, et al. TSPO PET with [18F]GE-180 sensitively detects focal neuroinflammation in patients with relapsing-remitting multiple sclerosis. *Eur J Nucl Med Mol Imaging*. 2018;45:1423-1431.

15. Radu CG, Shu CJ, Shelly SM, Phelps ME, Witte ON. Positron emission tomography with computed tomography imaging of neuroinflammation in experimental autoimmune encephalomyelitis. *Proc Natl Acad Sci U S A*. 2007;104:1937-1942.
16. James ML, Hoehne A, Mayer AT, et al. Imaging B cells in a mouse model of multiple sclerosis using ⁶⁴Cu-rituximab PET. *J Nucl Med*. 2017;58:1845-1851.
17. Gerwien H, Hermann S, Zhang X, et al. Imaging matrix metalloproteinase activity in multiple sclerosis as a specific marker of leukocyte penetration of the blood-brain barrier. *Sci Transl Med*. 2016;8:364ra152.
18. Radu CG, Shu CJ, Nair-Gill E, et al. Molecular imaging of lymphoid organs and immune activation by positron emission tomography with a new [¹⁸F]-labeled 2'-deoxycytidine analog. *Nat Med*. 2008;14:783-788.
19. Nair-Gill E, Wiltzius SM, Wei XX, et al. PET probes for distinct metabolic pathways have different cell specificities during immune responses in mice. *J Clin Invest*. 2010;120:2005-2015.
20. Salas JR, Chen BY, Wong A, et al. ¹⁸F-FAC PET selectively images liver-infiltrating CD4 and CD8 T cells in a mouse model of autoimmune hepatitis. *J Nucl Med*. 2018;59:1616-1623.
21. Miller SD, Karpus WJ. Experimental autoimmune encephalomyelitis in the mouse. *Curr Protoc Immunol*. 2007;Chapter 15:Unit 15.1.
22. Fedchenko N, Reifenrath J. Different approaches for interpretation and reporting of immunohistochemistry analysis results in the bone tissue - a review. *Diagn Pathol*. 2014;9:221.
23. Loening AM, Gambhir SS. AMIDE: a free software tool for multimodality medical image analysis. *Mol Imaging*. 2003;2:131-137.
24. Ma Y, Hof PR, Grant SC, et al. A three-dimensional digital atlas database of the adult C57BL/6J mouse brain by magnetic resonance microscopy. *Neuroscience*. 2005;135:1203-1215.
25. Barrio MJ, Spick C, Radu CG, et al. Human biodistribution and radiation dosimetry of ¹⁸F-clofarabine, a PET probe targeting the deoxyribonucleoside salvage pathway. *J Nucl Med*. 2017;58:374-378.
26. Salas JR, Chen BY, Wong A, et al. Noninvasive imaging of drug-induced liver injury with ¹⁸F-DFA PET. *J Nucl Med*. 2018;59:1308-1315.
27. LaFrance-Corey RG, Howe CL. Isolation of brain-infiltrating leukocytes. *J Vis Exp*. 2011.
28. Cansev M. Uridine and cytidine in the brain: their transport and utilization. *Brain Res Rev*. 2006;52:389-397.
29. Dai H, Marbach P, Lemaire M, Hayes M, Elmquist WF. Distribution of STI-571 to the brain is limited by P-glycoprotein-mediated efflux. *J Pharmacol Exp Ther*. 2003;304:1085-1092.

30. Pike VW. PET radiotracers: crossing the blood-brain barrier and surviving metabolism. *Trends Pharmacol Sci*. 2009;30:431-440.
31. Schmitt C, Strazielle N, Gherzi-Egea J-F. Brain leukocyte infiltration initiated by peripheral inflammation or experimental autoimmune encephalomyelitis occurs through pathways connected to the CSF-filled compartments of the forebrain and midbrain. *J Neuroinflammation*. 2012;9:187.
32. Brown DA, Sawchenko PE. Time course and distribution of inflammatory and neurodegenerative events suggest structural bases for the pathogenesis of experimental autoimmune encephalomyelitis. *J Comp Neurol*. 2007;502:236-260.
33. Bennett J, Basivireddy J, Kollar A, et al. Blood-brain barrier disruption and enhanced vascular permeability in the multiple sclerosis model EAE. *J Neuroimmunol*. 2010;229:180-191.
34. Toy G, Austin WR, Liao H-I, et al. Requirement for deoxycytidine kinase in T and B lymphocyte development. *Proc Natl Acad Sci U S A*. 2010;107:5551-5556.
35. Cohen JA, Chun J. Mechanisms of fingolimod's efficacy and adverse effects in multiple sclerosis. *Ann Neurol*. 2011;69:759-777.
36. Shu CJ, Campbell DO, Lee JT, et al. Novel PET probes specific for deoxycytidine kinase. *J Nucl Med*. 2010;51:1092-1098.
37. Schwarzenberg J, Radu CG, Benz M, et al. Human biodistribution and radiation dosimetry of novel PET probes targeting the deoxyribonucleoside salvage pathway. *Eur J Nucl Med Mol Imaging*. 2011;38:711-721.
38. Kim W, Le TM, Wei L, et al. [18F]CFA as a clinically translatable probe for PET imaging of deoxycytidine kinase activity. *Proc Natl Acad Sci U S A*. 2016;113:4027-4032.
39. Engvall C, Ryding E, Wirestam R, et al. Human cerebral blood volume (CBV) measured by dynamic susceptibility contrast MRI and 99mTc-RBC SPECT. *J Neurosurg Anesthesiol*. 2008;20:41-44.
40. Murphy JM, Armijo AL, Nomme J, et al. Development of new deoxycytidine kinase inhibitors and noninvasive in vivo evaluation using positron emission tomography. *J Med Chem*. 2013;56:6696-6708.
41. Calabresi PA, Radue E-W, Goodin D, et al. Safety and efficacy of fingolimod in patients with relapsing-remitting multiple sclerosis (FREEDOMS II): a double-blind, randomised, placebo-controlled, phase 3 trial. *Lancet Neurol*. 2014;13:545-556.
42. Brewer S, Nair-Gill E, Wei B, et al. Epithelial uptake of [18F]1-(2'-deoxy-2'-arabinofuranosyl) cytosine indicates intestinal inflammation in mice. *Gastroenterology*. 2010;138:1266-1275.

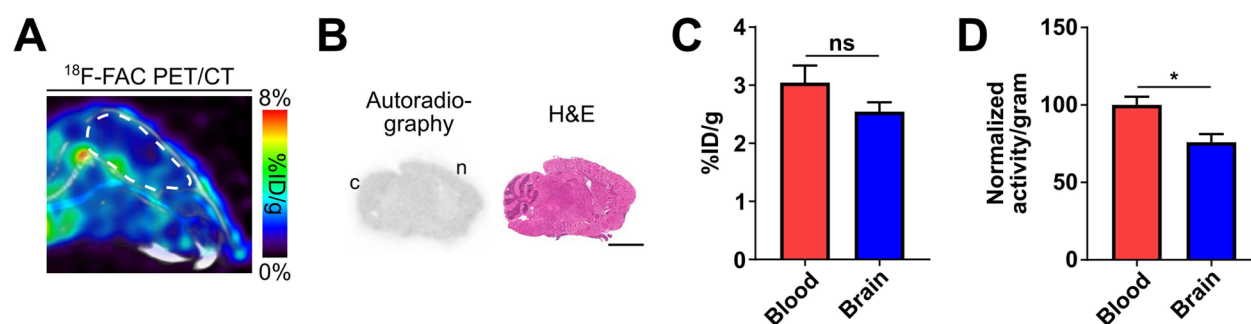


Figure 1. ^{18}F -FAC crosses the healthy BBB in mice. (A) Sagittal ^{18}F -FAC PET/CT image of a healthy C57BL/6 mouse. Representative image of $n=5$. Brain outlined in white. (B) ^{18}F -FAC autoradiography and H&E staining of a sagittal brain section from a healthy C57BL/6 mouse. Scale bar: 3 mm. c: cerebellum, n: neocortex. Representative image of $n=5$. (C) Blood and brain ^{18}F -FAC levels, quantified from PET images of healthy C57BL/6 mice. $n=5$. (D) Normalized blood and brain ^{18}F -FAC levels, quantified from extracted blood and brain. $n=6$. *: $P < 0.05$, ns: not significant.

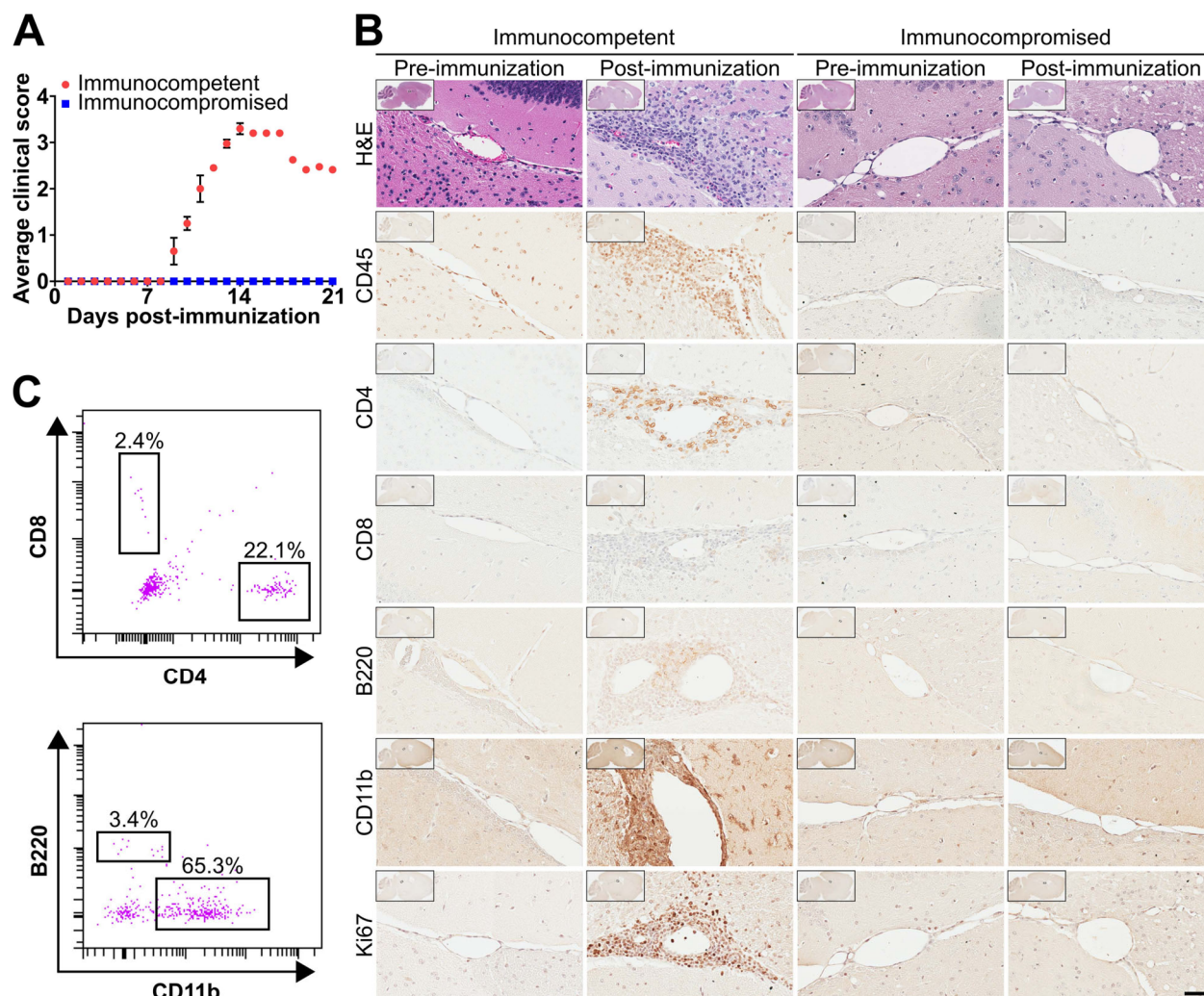


Figure 2. Brain-infiltrating leukocytes are present in a mouse model of EAE. (A) Time course of EAE symptoms in immunocompetent and immunocompromised mice. $n=4$. (B) H&E and immunohistochemical stains of brain sections of mice pre- and post-immunization. 1X and 40X magnification images. Scale bar: 50 microns. $n=2$. (C) Immune cell populations isolated by fluorescence-activated cell sorting from immunocompetent EAE mouse brains. $n=3$.

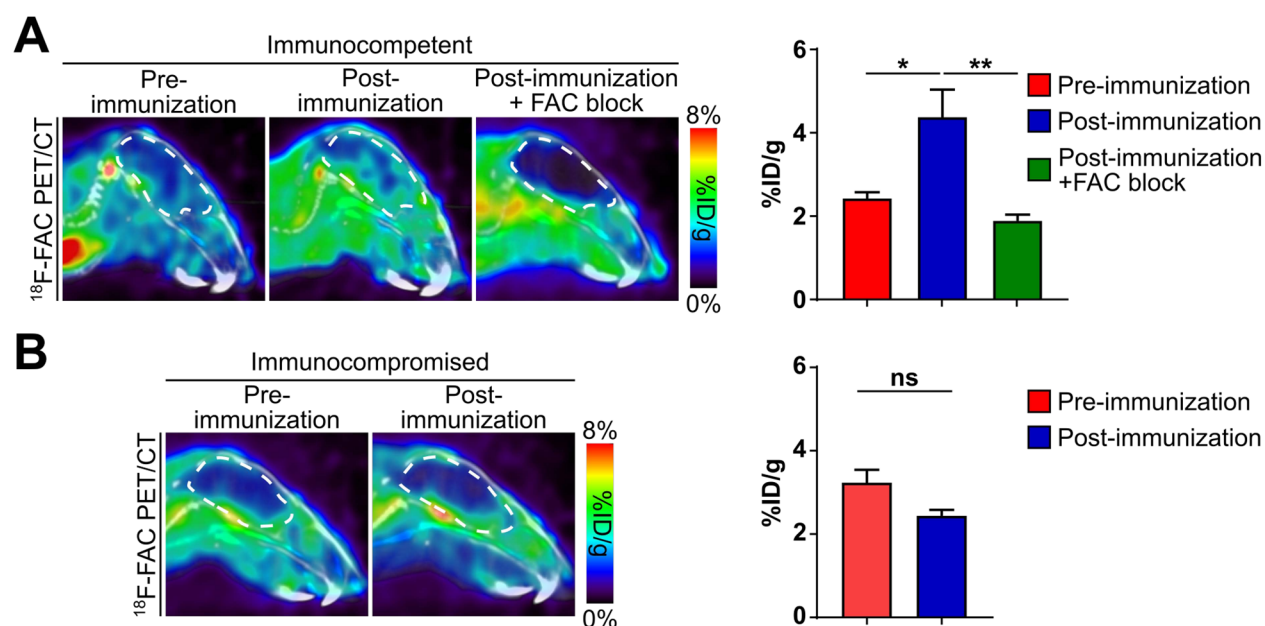


Figure 3. ^{18}F -FAC accumulates more in the brains of EAE mice than control mice. Sagittal ^{18}F -FAC PET/CT images (*left*) and quantification (*right*) of (A) immunocompetent and (B) immunocompromised pre- and post-immunization mice. FAC block: co-injection of mice with ^{18}F -FAC and non-radiolabeled FAC. All experiments: $n=4$. *: $P<0.05$, **: $P<0.01$, ns: not significant. Brains outlined in white.

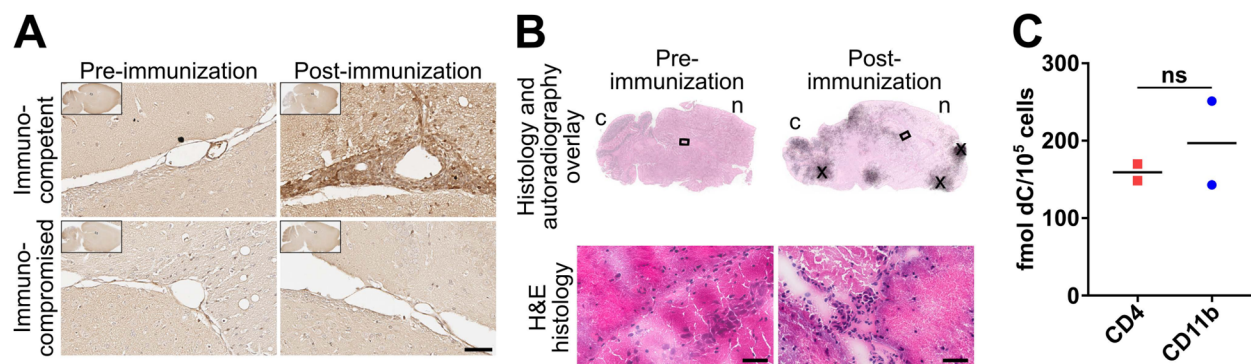


Figure 4. ^{18}F -FAC accumulates in brain-infiltrating leukocytes in an EAE mouse model. (A) Mouse brain sections immunostained for deoxycytidine kinase pre- and post-immunization. 1X and 40X magnification images. Scale bar: 50 microns. $n=2$. (B) ^{18}F -FAC autoradiography images and H&E staining of sagittal brain sections of immunocompetent mice pre- and post-immunization. 1X and 40X magnification images. Scale bars: 50 microns. c: cerebellum, n: neocortex, x: regions where the tissue wrinkled. $n=2$. (C) Deoxycytidine (dC) accumulation in leukocyte populations isolated from immunocompetent EAE mouse brains. $n=2$. ns: not significant.

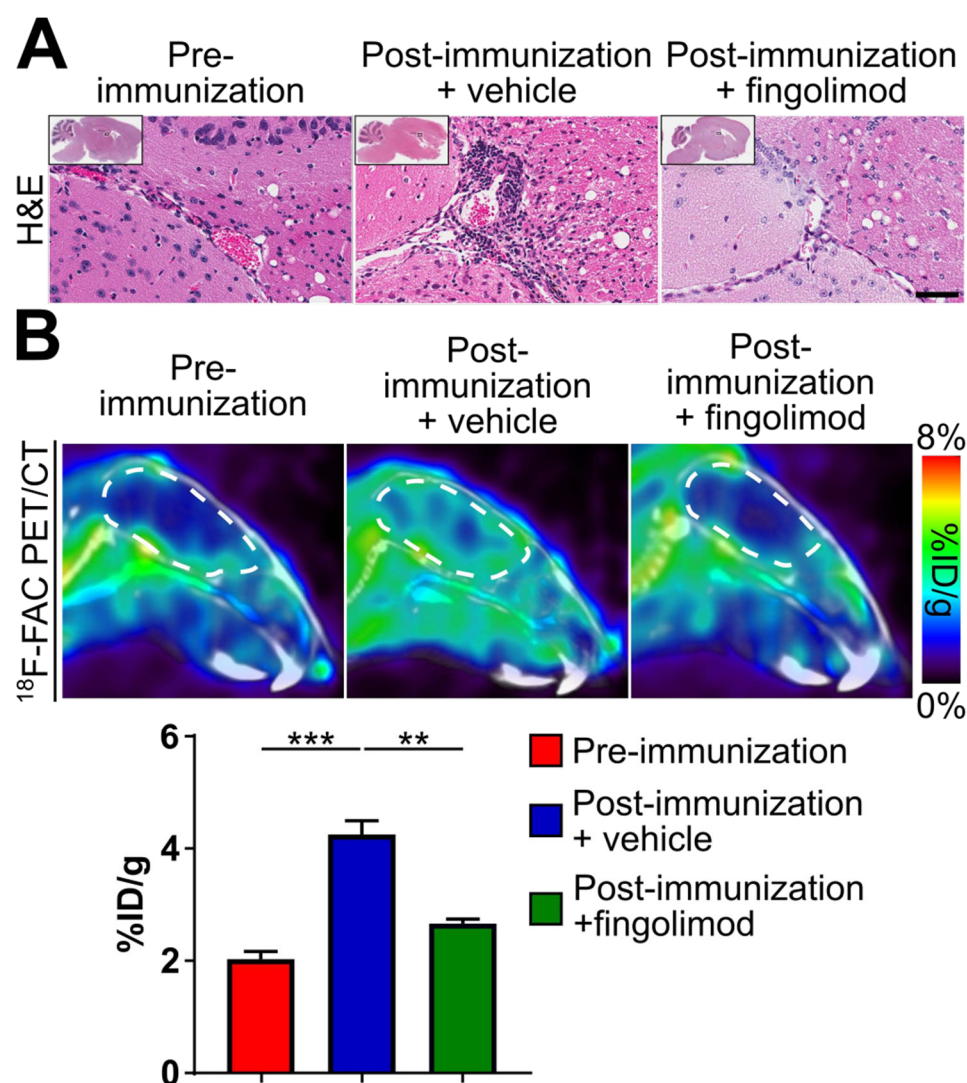


Figure 5. ^{18}F -FAC PET can monitor immunomodulatory drug treatments in an EAE mouse model. (A) H&E stains of brain sections and (B) sagittal PET/CT images and quantification of ^{18}F -FAC accumulation in the brains of mice pre-immunization, and post-immunization and treated with vehicle or fingolimod. 1X and 40X magnification images. Scale bar: 50 microns. H&E: $n=2$; PET/CT: Pre-immunization: $n=4$, Post-immunization + vehicle: $n=4$; Post-immunization + fingolimod: $n=3$. **: $P<0.01$, ***: $P<0.001$. Brains outlined in white.

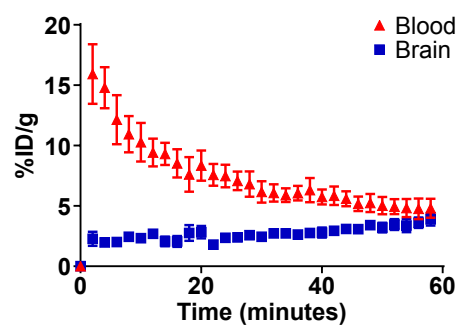
Supplemental information

^{18}F -FAC PET visualizes brain-infiltrating leukocytes in a mouse model of multiple sclerosis

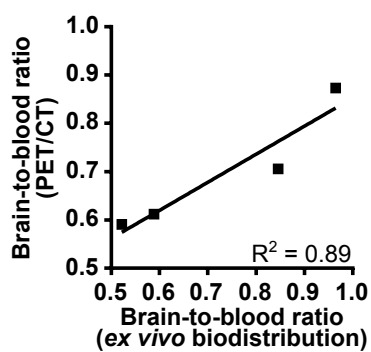
Bao Ying Chen^{1,2}, Chiara Ghezzi^{1,2}, Brendon Villegas³, Andrew

Quon^{1,4}, Caius G. Radu^{1,4}, Owen N. Witte^{1,5,6}, Peter M. Clark^{1,2,5}

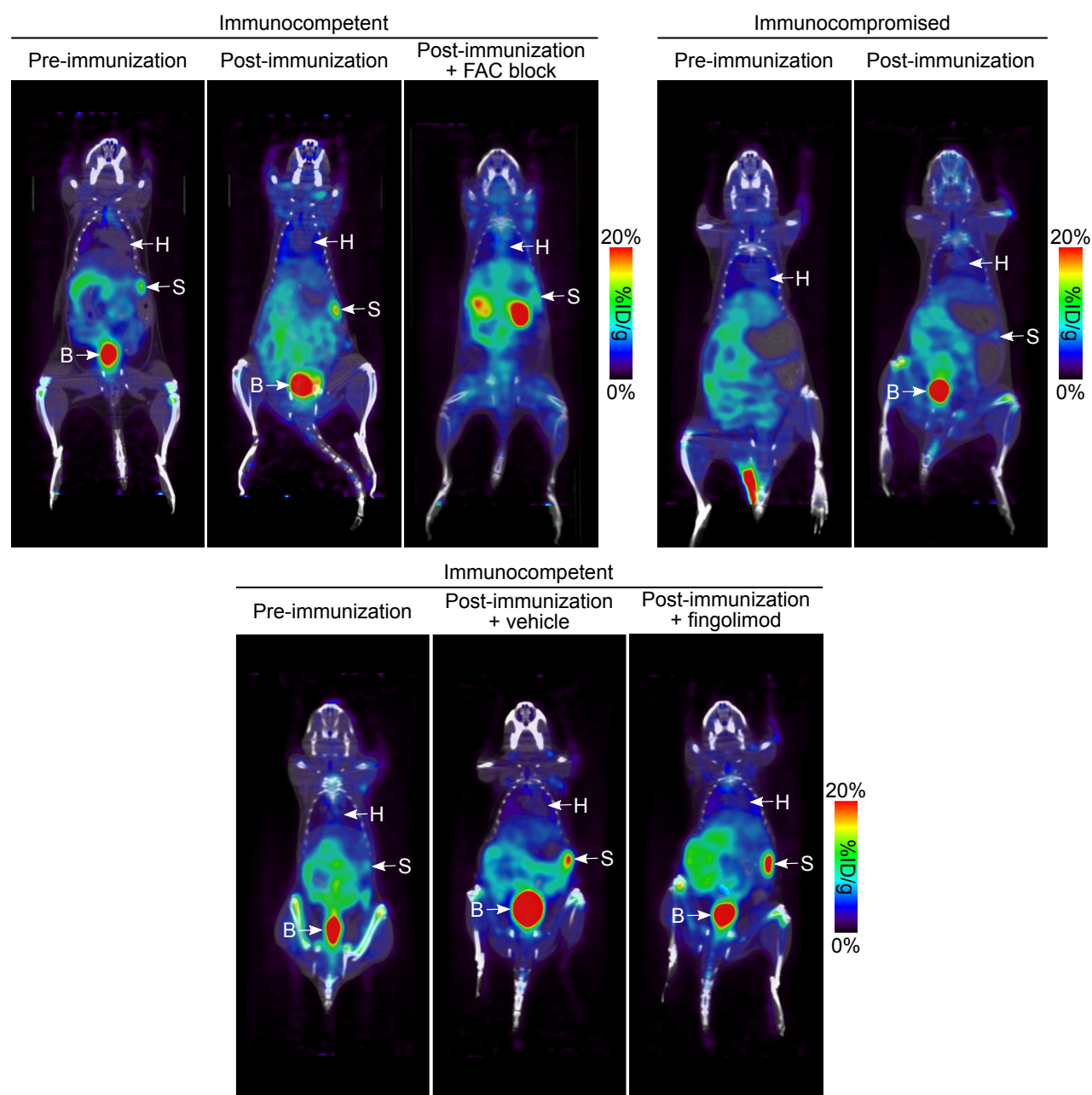
¹ Department of Molecular and Medical Pharmacology, ² Crump Institute for Molecular Imaging, ³ Department of Pulmonary and Critical Care Medicine, ⁴ Ahmanson Translational Imaging Division, ⁵ Eli and Edythe Broad Center of Regenerative Medicine and Stem Cell Research, ⁶ Department of Microbiology, Immunology, and Molecular Genetics, University of California, Los Angeles, CA 90095.



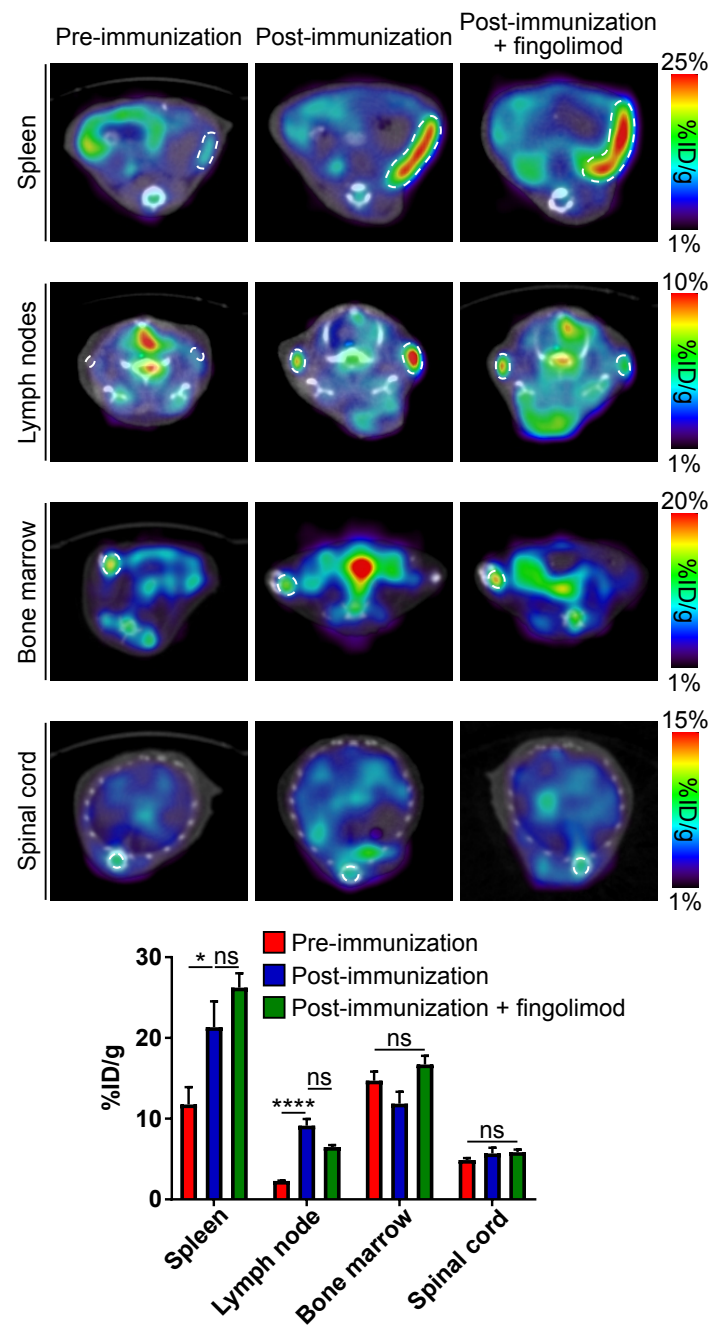
Supplemental Figure 1. Time-activity curves of ^{18}F -FAC accumulation in the blood and brains of healthy mice. $n=5$.



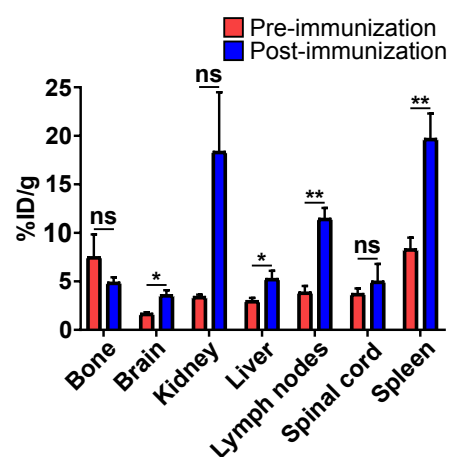
Supplemental Figure 2. Brain-to-blood ratios of ^{18}F -FAC in healthy mice, as measured from the PET/CT images and *ex vivo* biodistribution studies. $n=4$.



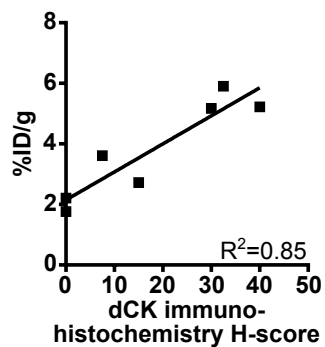
Supplemental Figure 3. ^{18}F -FAC accumulation in immunocompetent and immunocompromised mice pre- and post-immunization, and co-injected with non-radiolabeled FAC (FAC block) or treated with vehicle or fingolimod. H = heart, S = spleen, B = bladder.



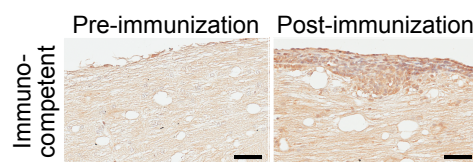
Supplemental Figure 4. ^{18}F -FAC PET can be used to monitor peripheral immune activation at specific locations throughout the body in EAE mice and following treatment with an immunomodulatory drug. Representative transverse ^{18}F -FAC PET/CT images of immunocompetent mice pre-immunization, post-immunization, and post-immunization and treated with fingolimod. Spleen, lymph nodes, bone marrow, and spinal cord encircled in a white dotted line (*top*). Quantification (*bottom*). Pre-immunization and post-immunization: $n=7$; post-immunization and treated with fingolimod: $n=3$. *: $P<0.05$; ****: $P<0.0001$, ns: not significant.



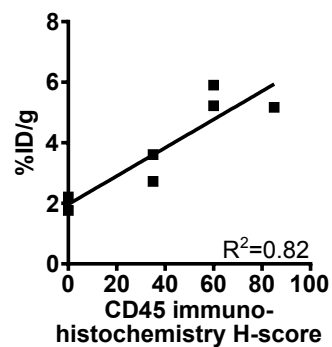
Supplemental Figure 5. ^{18}F -FAC biodistribution, measured *ex vivo* in organs from immunocompetent mice pre- and post-immunization. $n=4$ except for spinal cord which is $n=3$. *: $P<0.05$, **: $P<0.01$, ns: not significant.



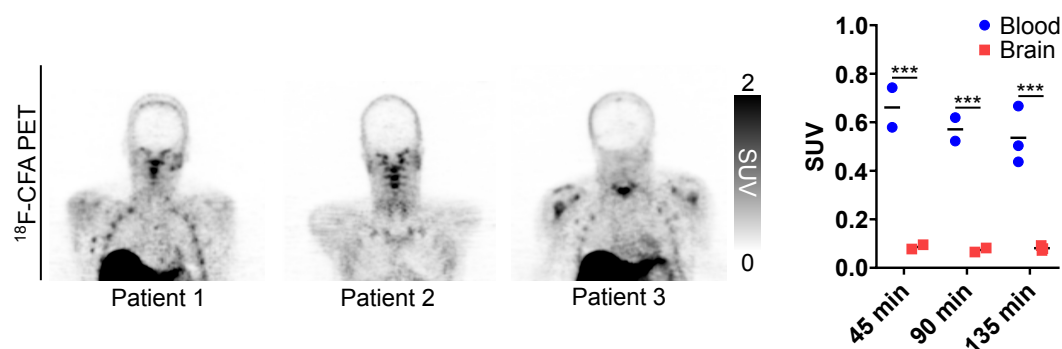
Supplemental Figure 6. dCK immunostaining (as measured by an immunohistochemistry H-score) and ^{18}F -FAC accumulation in the brains of immunocompetent mice. $n=7$.



Supplemental Figure 7. dCK immunostaining of spinal cord tissue sections from immunocompetent mice pre- and post-immunization. 40x magnification images. Scale bars: 50 microns. Representative images of $n=2$.



Supplemental Figure 8. CD45 immunostaining (as measured by an immunohistochemistry H-score) and ¹⁸F-FAC accumulation in the brains of immunocompetent mice. *n*=7.



Supplemental Figure 9. ^{18}F -CFA does not readily cross the blood-brain barrier in healthy human subjects. Representative coronal PET images of healthy volunteers injected with ^{18}F -CFA at 135 min post-tracer injection (*left*). Blood and brain ^{18}F -CFA accumulation, quantified from the PET images of healthy volunteers (*right*). The PET scans analyzed here are the same as those reported in Ref. 25. 45 and 90 min time point: $n=2$; 135 min time point: $n=3$. ***: $P<0.001$.



The Journal of
NUCLEAR MEDICINE

^{18}F -FAC PET visualizes brain-infiltrating leukocytes in a mouse model of multiple sclerosis

Bao Ying Chen, Chiara Ghezzi, Brendon Villegas, Andrew Quon, Caius G. Radu, Owen N. Witte and Peter M. Clark

J Nucl Med.

Published online: October 25, 2019.

Doi: 10.2967/jnumed.119.229351

This article and updated information are available at:

<http://jnm.snmjournals.org/content/early/2019/10/24/jnumed.119.229351>

Information about reproducing figures, tables, or other portions of this article can be found online at:

<http://jnm.snmjournals.org/site/misc/permission.xhtml>


Information about subscriptions to JNM can be found at:

<http://jnm.snmjournals.org/site/subscriptions/online.xhtml>

JNM ahead of print articles have been peer reviewed and accepted for publication in *JNM*. They have not been copyedited, nor have they appeared in a print or online issue of the journal. Once the accepted manuscripts appear in the *JNM* ahead of print area, they will be prepared for print and online publication, which includes copyediting, typesetting, proofreading, and author review. This process may lead to differences between the accepted version of the manuscript and the final, published version.

The Journal of Nuclear Medicine is published monthly.
SNMMI | Society of Nuclear Medicine and Molecular Imaging
1850 Samuel Morse Drive, Reston, VA 20190.
(Print ISSN: 0161-5505, Online ISSN: 2159-662X)

© Copyright 2019 SNMMI; all rights reserved.

 SOCIETY OF
NUCLEAR MEDICINE
AND MOLECULAR IMAGING